PHYSICAL REVIEW C VOLUME 46, NUMBER 3 SEPTEMBER 1992

# Phase-shift analysis of neutron-$^{208}$Pb scattering and mean-field studies

Z. P. Chen,* W. Tornow, and R. L. Walter
*Department of Physics, Duke University, Durham, North Carolina 27706*
*and Triangle Universities Nuclear Laboratory, Duke Station, Durham, North Carolina 27706*
(Received 23 December 1991)

The existing $n$-$^{208}$Pb elastic differential cross section, analyzing power, and total cross-section data in the energy range from 4 to 30 MeV were analyzed via a phase-shift analysis in order to find out how well these data are suited for dispersion relation based mean-field studies. It was found that the data can be well described by the phase-shift method and that overlapping resonances are likely to be responsible for deviations between the data and the fits obtained in recent optical-model analyses using the dispersion relation approach.

PACS number(s): 25.40.Dn, 24.10.−i, 24.30.Gd

## I. INTRODUCTION

The nuclei $^{40}$Ca and $^{208}$Pb have been widely considered as the favorite testing ground in nuclear structure and reaction studies. As a consequence, a wealth of data has been accumulated for these spherical nuclei. It is therefore not surprising that low-energy $n$-$^{208}$Pb elastic scattering data have been used recently [1–3] for guiding the extension of the optical-model potential determined at positive energies to the negative energy regime of the shell-model potential. This extension is based on the dispersion relation connecting the real and imaginary parts of the nucleon-nucleus potential [4]. This approach allows detailed calculations of single-particle energies, rms radii, occupation probabilities of single-particle orbits, and spectroscopic factors and spectral functions of single-particle excitations [1].

Since the dispersion relation incorporates more basic physics (causality) than the conventional optical-model approach, one would expect a more accurate description of nucleon-nucleus scattering data than previously obtained in conventional analyses. Somewhat surprisingly, it turned out that this expectation was wrong. Although the fits obtained in the $n$-$^{208}$Pb mean-field studies of Refs. [1–3] of the differential cross section $\sigma(\theta)$ data from Ohio University [5–7], Triangle Universities Nuclear Laboratory (TUNL) [8], and Michigan State University [9] are generally good, disturbing differences exist between the model prediction and the data. The inclusion of new TUNL analyzing power $A_y(\theta)$ data [3] to the database did not improve the situation appreciably, nor did the introduction of an angular-momentum dependence of the imaginary part of the nuclear mean field [1]. Fourier-Bessel-type optical-model analyses revealed that almost perfect fits can be obtained, if one allows for a somewhat erratic energy dependence of the associated parameters and potential shapes [10]. Therefore, suspicion grew that the $n$-$^{208}$Pb database may not be as ideal as generally assumed.

To investigate this suspicion, we performed a phase-shift analysis of the available $\sigma(\theta)$, $A_y(\theta)$, and total cross-section $\sigma_{tot}$ data for $n$-$^{208}$Pb in the energy range 4–30 MeV. Although a large number of parameters is required for describing this system, it is expected that the energy dependence of the phase-shift parameters can be more accurately interpreted than the results obtained from a Fourier-Bessel analysis, which requires about the same number of parameters.

## II. PHASE-SHIFT ANALYSIS RESULTS FOR $n$-$^{208}$Pb

Starting from the smooth phase-shift parameters determined from the spherical optical model obtained in the analysis for $n$-$^{208}$Pb by Roberts *et al.* [3], we first searched on the phase shifts in the 4–10 MeV energy range. In order to avoid erratic changes in the phase-shift parameters, we allowed only for smooth variations of the phase shifts. Of course, this constraint affected the quality of the fits on a $\chi^2$ basis; on the other hand, however, it reduced the possibility that the fitting program might have tried to account for some irregularities in the data which may be unphysical. After time-consuming tests were made to make sure that the present analysis between 4 and 10 MeV is most likely unique, we extended the phase-shift analysis up to 30 MeV.

The maximum number of partial waves used in the phase-shift search at a given energy was taken from the optical-model analysis of Ref. [3]. We included only partial waves with real part phase-shift values larger than 0.1°. Initially, the normalization of the $\sigma(\theta)$, $A_y(\theta)$, and total cross-section $\sigma_{tot}$ data was set to 1.0. After the first

*Permanent address: Tsinghua University, Beijing, The People's Republic of China.

 

search, the calculated best normalization factors were employed for all following searches. The final normalization factors were between 0.97 and 1.03, in agreement with the experimental normalization uncertainties for $A_y(\theta)$ and $\sigma_{\rm tot}$.

Figures 1 and 2 show fits obtained for the $\sigma(\theta)$ data in the 4–30 MeV energy range. Figure 3 presents fits to the available $A_y(\theta)$ data, and Fig. 4 gives our description of the total $n$-$^{208}$Pb cross section in the energy range of interest. In general, the agreement between data and fits is very good. A short glance at these figures does not indicate that resonances play a substantial role in the $n$-$^{208}$Pb scattering system at these energies. However, inspection of the phase-shift parameters and their energy dependence reveals that the $n$-$^{208}$Pb system is influenced by overlapping resonancelike structures. Figures 5–8 display the real part $\delta$ and the absorptive part $\eta$ of the phase shifts obtained in the present analysis for orbital angular momenta $l=0$ ($s$ wave) to $l=8$ ($k$ wave). Altogether, $l$ values up to $l=14$ were included in the analysis. As can be seen, the phase shifts deviate considerably from a smooth energy dependence. The uncertainties assigned to the phase-shift parameters were obtained from the relation

$$\chi^2(p+\Delta p)/\chi^2(p)=1+1/(N+1)^{1/2} . \tag{1}$$

Here, $p$ is the value of the best-fit parameter obtained in the best fit, $\Delta p$ is the associated uncertainty and $N$ is the number of parameters varied. In order to obtain $\Delta p$, we changed the value of $p$ in small steps (the other parameters were kept constant) and calculated the individual $\chi^2(p+\Delta p)$ values until Eq. (1) was fulfilled. Contrary to the relative normalization, it is very difficult to accurately determine the absolute normalization uncertainty of $\sigma(\theta)$ data. Therefore, we arbitrarily changed the absolute normalization of the $\sigma(\theta)$ data by as much as 10% to investi-

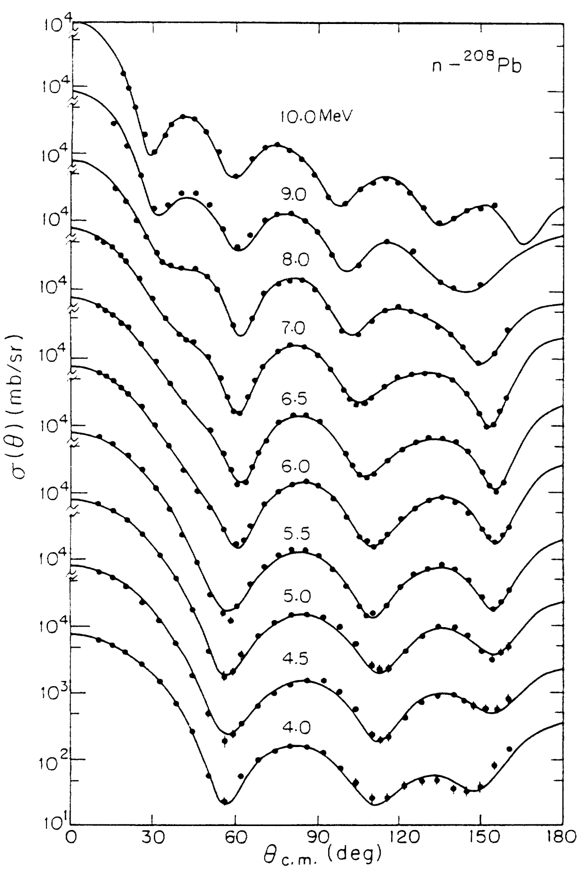


FIG. 1. Comparison of phase-shift analysis results (solid curves) and differential cross-section $\sigma(\theta)$ data for $n$-$^{208}$Pb between 4 and 10 MeV. The data between 4 and 7 MeV were measured at Ohio University (Annand *et al.* [5]). The data at 8 MeV are from TUNL (Roberts *et al.* [3]) and the data at 9 and 10 MeV were measured at Ohio University (Rapaport *et al.* [6]) and TUNL (Floyd *et al.* [8]), respectively.

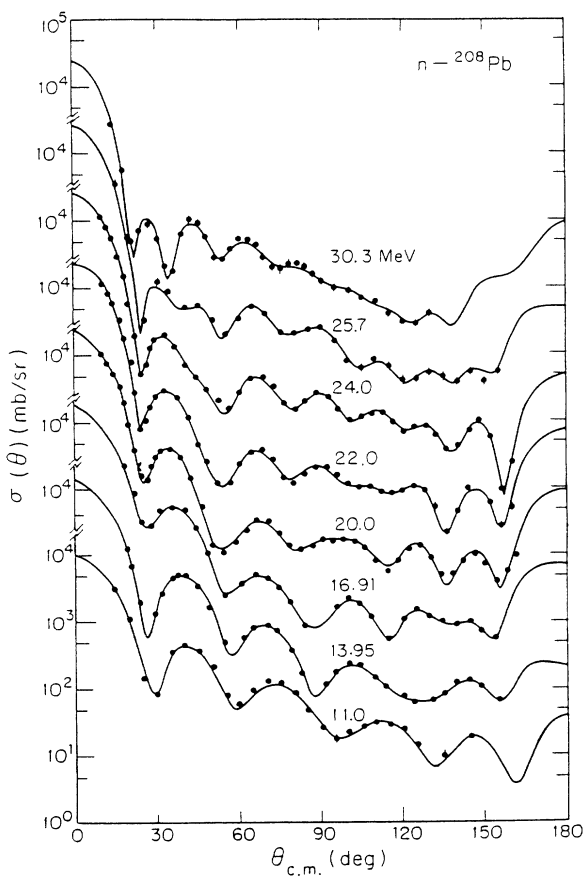


FIG. 2. Comparison of phase-shift analysis results (solid curves) and differential cross-section data for $n$-$^{208}$Pb between 11 and 30.3 MeV. The data at 11 and 25.7 MeV are from Ohio University (Rapaport *et al.* [6]). The data at 13.95 and 16.91 MeV were measured at TUNL (Floyd *et al.* [8]). The data at 20, 22, and 24 MeV are from Ohio University (Finlay *et al.* [7]) and the data at 30.3 MeV were measured at Michigan State University (DeVito *et al.* [9]).

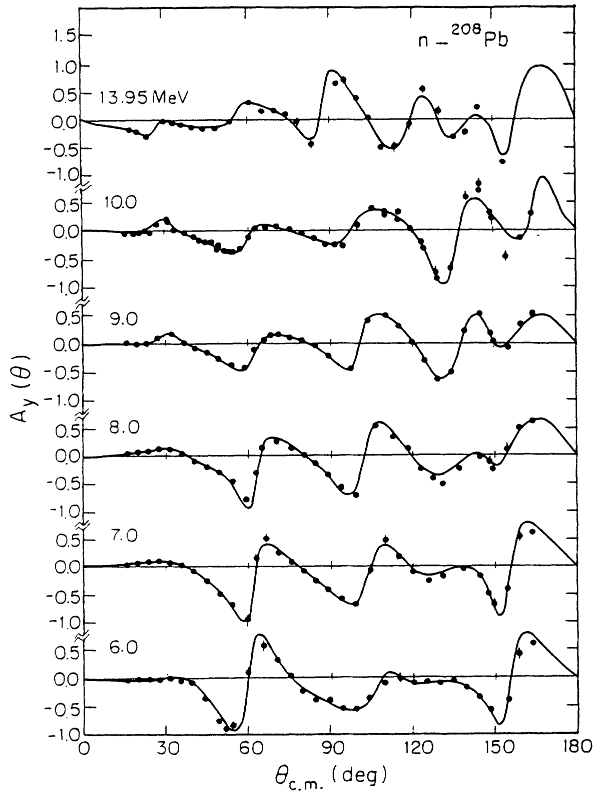


FIG. 3. Comparison of phase-shift analysis results (solid curves) and analyzing power $A_y(\theta)$ data obtained at TUNL for $n$-$^{208}$Pb between 6 and 13.95 MeV. The data between 6 and 9 MeV were measured by Roberts *et al.* [3]. The data at 10 MeV are from Floyd *et al.* [8] and Roberts *et al.* [3] and the data at 13.95 MeV are from Floyd *et al.* [8].

TABLE I. Resonance parameters for $n$-$^{208}$Pb.

| $E_{nR}$ (MeV) | $E_x$ (MeV) | $J^\pi$ | $\Gamma$ (MeV) | $\Gamma_n/\Gamma$ |
|---|---|---|---|---|
| 3.8 | 7.7 | $3/2^-$ | 1.1 | 0.27 |
| 5.9 | 9.8 | $3/2^+$ | 0.6 | 0.19 |
| 5.9 | 9.8 | $9/2^+$ | 0.6 | 0.06 |
| 6.3 | 10.2 | $5/2^-$ | 1.5 | 0.21 |
| 6.4 | 10.3 | $11/2^-$ | 1.0 | 0.15 |
| 7.9 | 11.8 | $7/2^-$ | 1.8 | 0.56 |
| 9.1 | 13.0 | $1/2^+$ | 1.5 | 0.74 |
| 9.5 | 13.4 | $5/2^+$ | 4.7 | 1.00 |
| 9.6 | 13.5 | $13/2^-$ | 1.9 | 0.34 |
| 10.1 | 14.0 | $3/2^-$ | 1.8 | 0.69 |
| 10.4 | 14.3 | $1/2^-$ | 1.1 | 0.26 |
| 10.6 | 14.5 | $3/2^+$ | 1.6 | 0.35 |
| 14.1 | 18.0 | $11/2^+$ | 1.3 | 0.32 |
| 16.0 | 19.9 | $7/2^+$ | 3.4 | 0.85 |
| 16.6 | 20.5 | $15/2^+$ | 2.0 | 0.71 |
| 19.1 | 22.9 | $9/2^-$ | 2.9 | 0.89 |
| 20.2 | 24.0 | $3/2^+$ | 1.3 | 0.21 |
| 20.3 | 24.1 | $5/2^-$ | 1.3 | 0.12 |
| 23.8 | 27.6 | $13/2^-$ | 2.9 | 0.39 |
| 26.1 | 29.9 | $11/2^-$ | 1.2 | 0.16 |
| 26.8 | 30.6 | $9/2^+$ | 2.0 | 0.31 |

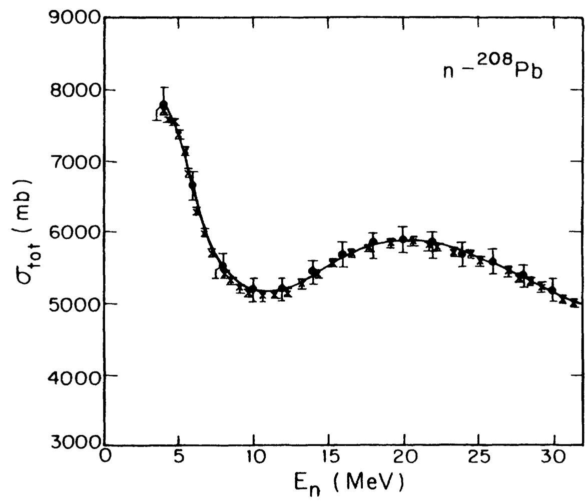


FIG. 4. Comparison of phase-shift analysis (solid curve) and $n$-$^{208}$Pb total cross section data from Larson *et al.* [11] (solid dots) and Schutt *et al.* [12] (crosses).

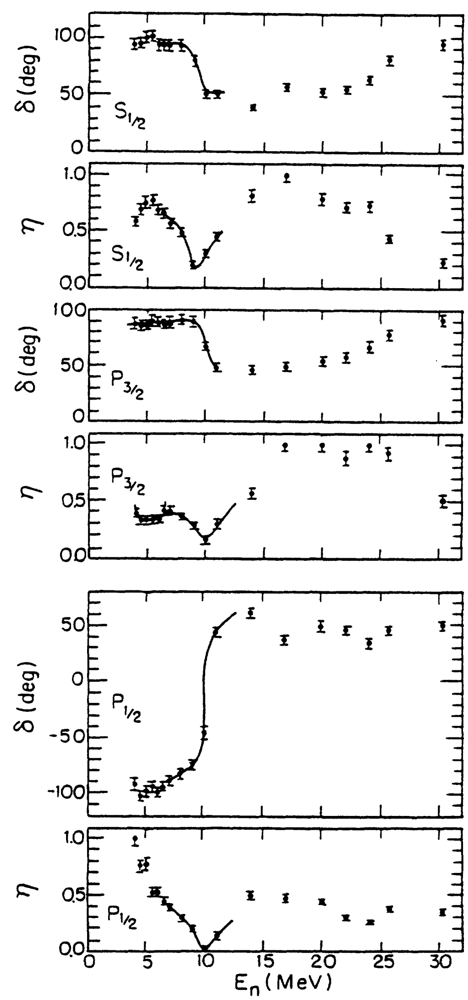


FIG. 5. Energy dependence of the $S_{1/2}$, $P_{3/2}$, and $P_{1/2}$ phase-shift parameters $\delta$ (real part) and $\eta$ (absorptive part) for $n$-$^{208}$Pb. The solid curves represent fits to the resonances identified in the present work.

gate whether the resonance structures can be smoothed out by renormalization. [The accurate $\sigma_{\mathrm{tot}}$ data prohibit a renormalization of $\sigma(\theta)$ as large as this.] In no case did the structures disappear.

The solid curves in Figs. 5–8 were obtained from fits to the "resonances" using the procedure outlined in Ref. [13]. The $S$-matrix elements were expressed using the relation [14]

$$S(E)=\eta\exp(2i\delta)=\exp(2i\phi_B)\{|B|+\exp(i\alpha)(\Gamma_n/\Gamma)[\exp(2i\beta)-1]\}\ . \tag{2}$$

Here, $|B|\exp(2i\phi_B)$ describes the background phase shift. The mixing angle $\alpha$ takes into account the relative phase between a resonance and the background phase. $\Gamma_n$ is the partial width of a resonance in the elastic channel and $\Gamma$ is its total width. The quantity $\beta=\tan^{-1}[\frac{1}{2}\Gamma/(E_{nR}-E)]$ denotes the resonance phase shift with $E_{nR}$ being the resonance energy. For 21 resonancelike structures the neutron energy $E_{nR}$, excitation energy $E_x$, $J^\pi$ values, total width $\Gamma$, and partial width

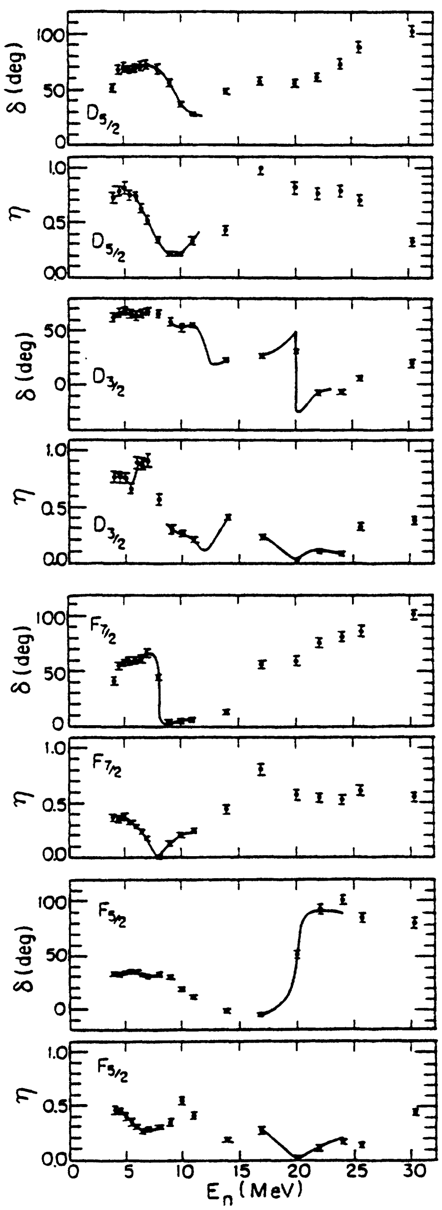


FIG. 6. Same as Fig. 5 for the $D_{5/2}$, $D_{3/2}$, $F_{7/2}$, and $F_{5/2}$ phase-shift parameters.

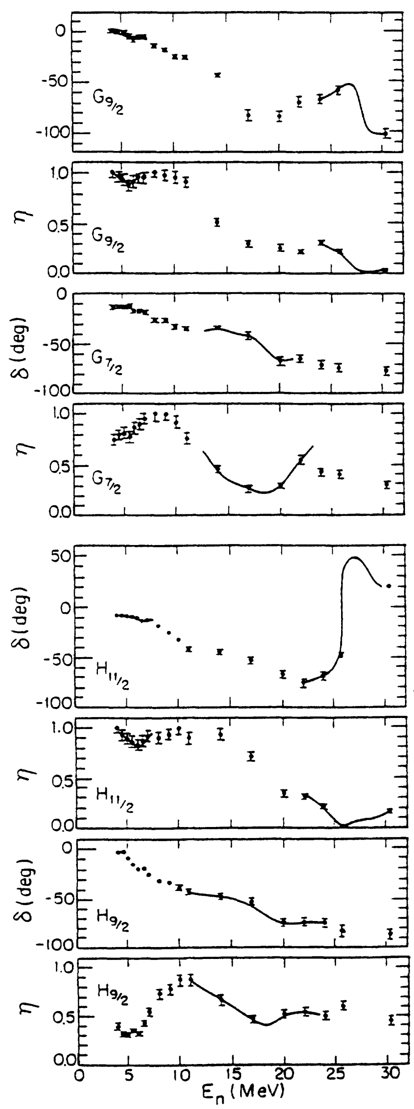


FIG. 7. Same as Fig. 5 for the $G_{9/2}$, $G_{7/2}$, $H_{11/2}$, and $H_{9/2}$ phase-shift parameters.

TABLE II. Threshold energies (in MeV) for some neutron-induced reactions on $^{208}$Pb and $^{209}$Bi. The $(n,\gamma)$, $(n,{}^4\text{He})$, and $(n,n{}^4\text{He})$ thresholds for $^{208}$Pb and $^{209}$Bi are negative.

| Reaction | $^{208}$Pb | $^{209}$Bi |
|---|---|---|
| $(n,p)$ | 4.23 | −0.13 |
| $(n,d)$ | 5.82 | 1.59 |
| $(n,t)$ | 6.41 | 2.70 |
| $(n,{}^3\text{He})$ | 7.70 | 4.12 |
| $(n,np)$ | 8.06 | 3.82 |

$\Gamma_n/\Gamma$ have been tentatively identified. Table I summarizes our results. Until now, no experimental information about states located in the high excitation energy range covered by our analysis has been published.

Figure 9 displays the Argand plots of the resonancelike structures observed in the present work. Ideally, counter-clockwise (with increasing energy) and closed circles are expected for isolated and narrow resonances. Except for a few cases, the "circles" found here are far from being closed. Since the resonancelike structures under discussion are fairly broad, the background phase shifts prevent the resonance circles from closing.

The origin of the unexpected resonancelike structures found in the $n$-$^{208}$Pb system is presently not understood. The "low-lying resonances" at $E_{nR}=3.8$, 5.9, 6.3, 6.4, and 7.9 MeV might be caused by cusp effects related to the opening of inelastic channels. Table II (left-hand side) gives the threshold energies for the $(n,p)$, $(n,d)$, $(n,t)$, $(n,{}^3\text{He})$, and $(n,np)$ reactions on $^{208}$Pb for transitions to the ground states of the associated residual nuclei. Since the level density of the residual nuclei of interest is large and the average level width is small compared to both the neutron energy spread employed in the experiments and the widths of the resonancelike structures, it is impossible to study reaction channels that lead to specific excited states of the residual nuclei. One might also speculate that the resonancelike structures are related to the doubly-closed shell nature of $^{208}$Pb. Contrary to the larger number of possible configurations available in non-doubly-closed shell nuclei, $^{208}$Pb might not be a good representation of a mean field as other nuclei and many-body effects might well be responsible for the formation of the structures observed in the present work. In order to check on this interpretation we plan over the next year to perform a similar phase-shift analysis for the $n$-$^{209}$Bi system for which a comparable set of $\sigma(\theta)$ data exists. Such an analysis will also be important for studying the influence of threshold effects. As can be seen from the comparison of columns 2 and 3 of Table II, the inelastic thresholds of interest for neutron-induced reactions of $^{208}$Pb and $^{209}$Bi are quite different.

Although additional data in smaller energy steps are needed to establish the resonance parameters with greater confidence, it is evident that the $n$-$^{208}$Pb system is characterized by broad overlapping resonancelike structures. Such "resonances" are not included in the mean-field formalism of the dispersion relation optical model. Therefore, it is not surprising that mean-field analyses (disper-

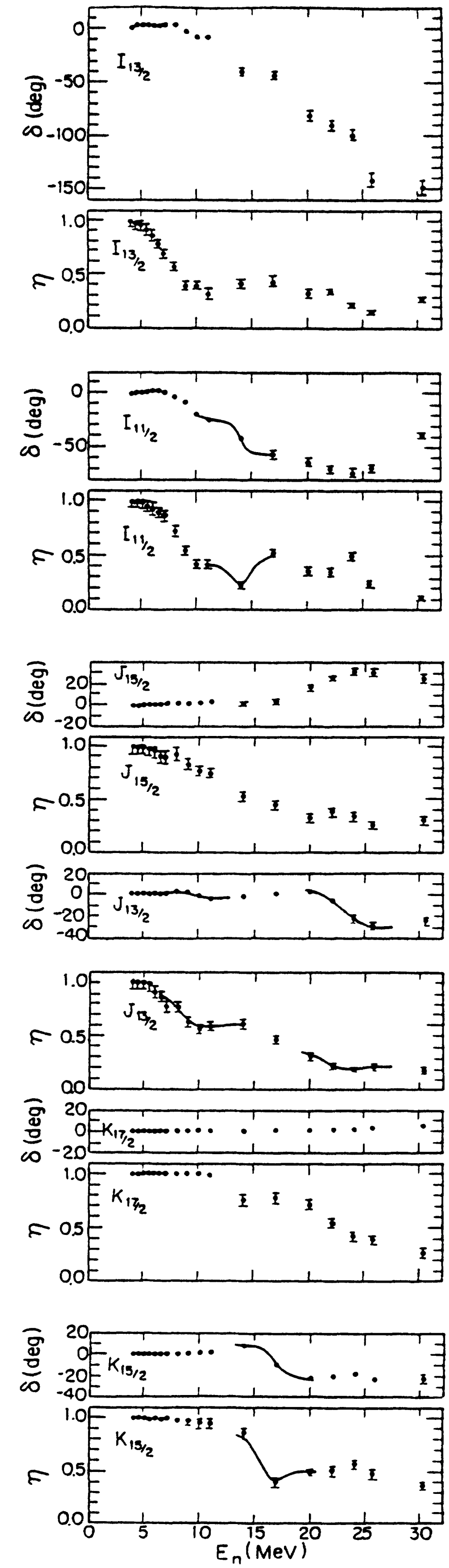


FIG. 8. Same as Fig. 5 for the $I_{13/2}$, $I_{11/2}$, $J_{15/2}$, $J_{13/2}$, $K_{17/2}$, and $K_{15/2}$ phase-shift parameters.

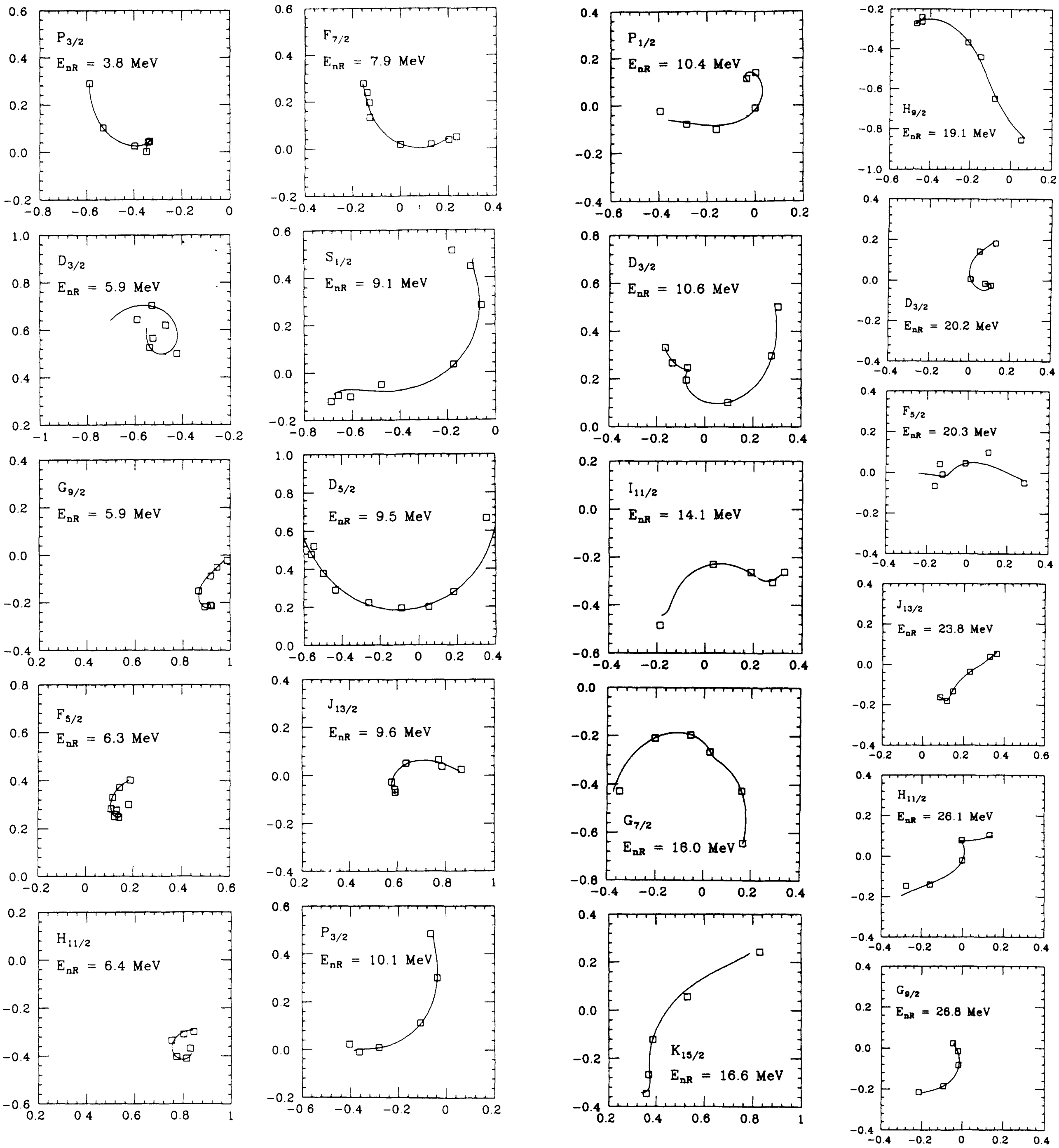


FIG. 9. Argand plots of the S-matrix elements. The horizontal and vertical axes represent the real and imaginary parts of the S-matrix elements. The squares were obtained from the phase-shift analysis. The solid curves are fits calculated from Eq. (2).

sive optical model [1,3] and iterative moment approach [2]), and the more conventional analyses as well, do not describe the experimental data as accurately as anticipated.

This work was supported in part by the U.S. Department of Energy, Office of High Energy and Nuclear Physics, under Contract No. DE-AC05-76ER01067.

[1] C. H. Johnson, D. J. Horen, and C. Mahaux, Phys. Rev. C **36**, 2252 (1987).
[2] C. Mahaux and R. Sartor, Nucl. Phys. **A516**, 285 (1990), and references therein.
[3] M. L. Roberts, P. D. Felsher, G. J. Weisel, Z. M. Chen, C. R. Howell, W. Tornow, R. L. Walter, and D. J. Horen, Phys. Rev. C **44**, 2006 (1991).
[4] I. Ahmad and W. Haider, J. Phys. G **2**, L157 (1976).
[5] J. R. M. Annand, R. W. Finlay, and F. S. Dietrich, Nucl. Phys. **A443**, 249 (1985).
[6] J. Rapaport, T. S. Cheema, D. E. Bainum, R. W. Finlay, and J. D. Carlson, Nucl. Phys. **A296**, 95 (1978).
[7] R. W. Finlay, J. R. M. Annand, T. S. Cheema, and J. Rapaport, Phys. Rev. C **30**, 796 (1984).
[8] C. E. Floyd, Ph.D. thesis, Duke University, 1981.
[9] R. P. DeVito, Ph.D. Dissertation, Michigan State University, 1979.
[10] M. L. Roberts, Ph.D. Dissertation, Duke University, 1988.
[11] D. C. Larson, private communication.
[12] R. L. Schutt, R. E. Shamu, P. W. Lisowski, M. S. Moore, and G. L. Morgan, Phys. Lett. B **203**, 22 (1988).
[13] W. Tornow, J. Phys. G **9**, 1507 (1983), and references therein.
[14] K. W. McVoy, in *Fundamentals in Nuclear Theory,* edited by A. De-Shalit and C. Villi (IAEA, Vienna, 1967), p. 419.